

Supplementary Information for

**Experimental and Theoretical Investigation of Overall Energy  
Deposition in Surface-Induced Unfolding of Protein Ions**

Micah T. Donor,<sup>a</sup> Austin M. Mroz,<sup>a</sup> and James S. Prell<sup>a,b\*</sup>

<sup>a</sup>Department of Chemistry and Biochemistry, 1253 University of Oregon,  
Eugene OR 97403-1253

<sup>b</sup>Materials Science Institute, University of Oregon, 1252 University of Oregon,  
Eugene, OR 97403-1252

\*Correspondence should be addressed to [jprell@uoregon.edu](mailto:jprell@uoregon.edu)

Tel: +1 (541) 346-2597

Fax: +1 (541) 346-4643

Table of Contents	<u>Page</u>
<b>Figure S1.</b> Additional CIU and SIU plots	S-3
Details of Monte Carlo modeling of CIU	S-4
Derivation of analytic expression for energy deposition in CIU without cooling	S-6
Derivation of model of collisional activation including both heating and cooling	S-8
<b>Figure S2.</b> Computed overall CIU efficiency vs. mass	S-10
<b>Figure S3.</b> Comparison of overall CIU efficiency for Monte Carlo simulations and theoretical model and effect of traveling wave	S-11
<b>Figure S4.</b> Dependence of computed CIU efficiency on CCS	S-12
<b>Figure S5.</b> Computed CIU efficiency of experimentally-observed conformer families of $\text{Mg}^{7+}$ , $\text{LFN}^{10+}$ , and $\text{BSA}^{15+}$	S-13
<b>Figure S6.</b> Residuals from fitted trend of SIU vs. CIU nominal energies plotted against various physical characteristics	S-14
<b>Figure S7.</b> Plot of nominal SIU energy vs. calibrated CIU energy using heating only model	S-15
<b>Figure S8.</b> In-source CIU fingerprint of $\text{BSA}^{15+}$	S-16
<b>Figure S9.</b> SIU of $\text{BSA}^{15+}$ with Trap pre-activation	S-17
<b>Figure S10.</b> CIU and SIU of $\text{TF}^{18+}$ with in-source pre-activation	S-18
<b>Figure S11.</b> Effective mass of surface	S-19

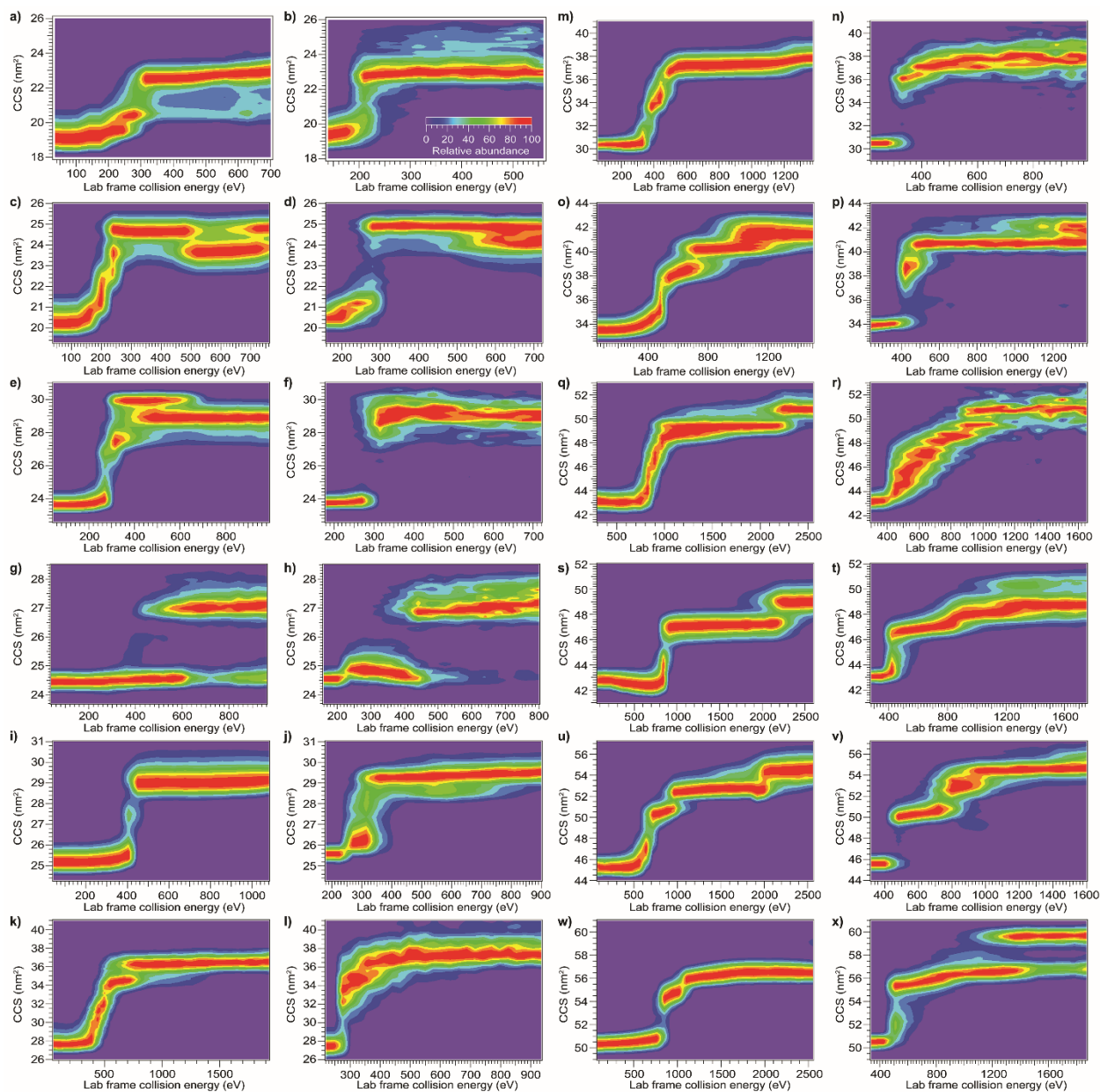


**Figure S1.** CIU and SIU plots, respectively, for **a)** and **b)** myoglobin, 7+ **c)** and **d)**  $\beta$ -lactoglobulin, 8+ **e)** and **f)** concanavalin A, 8+ **g)** and **h)** carbonic anhydrase 8+ **i)** and **j)** carbonic anhydrase 9+ **k)** and **l)** LF<sub>N</sub>, 11+ **m)** and **n)** alcohol dehydrogenase, 11+ **o)** and **p)** albumin, 12+ **q)** and **r)** PA<sub>63</sub>, 15+ **s)** and **t)** bovine serum albumin, 14+ **u)** and **v)** bovine serum albumin, 16+ **w)** and **x)** transferrin, 17+

### Monte Carlo modeling of CIU in a Synapt G2-Si

The initial kinetic energy of the ion was calculated as  $z \times V$ , where  $z$  is the charge on the ion and  $V$  the “Trap Collision Energy”, the voltage difference between the entrance electrode of the Trap and the exit electrode of the quadrupole.  $V$  was varied from 10 V to 200 V in steps of 5V for each protein. The traveling wave velocity in the simulations was 300 m/s, the wave height 2 V, and the wavelength 1.21 cm. The length of the collision cell in our modified instrument is 9 cm. The time step for each computation was

$$t_s = \frac{1}{20} \frac{mfp}{\sqrt{\frac{2 \times z \times 200}{m_i}}} \quad (1)$$

or  $1/20^{\text{th}}$  of the mean time between collisions for the maximum initial kinetic energy, where  $mfp$  is the mean free path and  $m_i$  is the mass of the ion. While the distance traveled was less than the length of the collision cell, for each time step the total distance traveled was computed as the velocity of the ion multiplied by the time step and the distance in the forward direction computed as the velocity in the forward direction multiplied by the time step. To determine if a collision occurred during the time step, a Monte Carlo sampling procedure was used. A random number between 0 and 1 was chosen, if it was smaller than the collision probability, calculated as  $1 - e^{-d_{ts}/mfp}$ , where  $d_{ts}$  is the total distance traveled during that time step, then a collision occurred. If a collision occurred, the distance traveled before the collision was determined as

$$d_c = -mfp \ln \left( r \left( 1 - e^{-\frac{d_{ts}}{mfp}} \right) + e^{-\frac{d_{ts}}{mfp}} \right) \quad (2)$$

where  $r$  is the random number used to determine that a collision occurred. The forward distance before the collision was

$$d_{c,z} = d_c \frac{d_{ts,z}}{d_{ts}} \quad (3)$$

To determine the geometry of the collision, the cosine of the polar angle (i.e.  $z$ -component of the unit velocity vector of the gas) was sampled from a uniform distribution from -1 to 1, the azimuthal angle was sampled from a uniform distribution from 0 to  $2\pi$ , and the  $x$ - and  $y$ -components of the gas vector determined as  $\cos(\Phi) \times \sin(\cos^{-1}(z))$  and  $\sin(\Phi) \times \sin(\cos^{-1}(z))$ , respectively. The gas velocity was sampled from a Maxwell-Boltzmann distribution

$$p(v) = \left( \frac{m_g}{2\pi k_b T} \right)^{\frac{3}{2}} 4\pi v^2 e^{-m_g v^2 / 2k_b T_g} \quad (4)$$

where  $m_g$  is the mass of the gas (Argon),  $k_b$  is the Boltzmann constant, and  $T_g$  is the temperature of the gas (298 K). The change in velocity due to the traveling wave potential was determined by computing the potential difference over the course of the time

$$\Delta V_{TW} = \frac{wh}{2} (\sin(kd_f - \omega t_f) - \sin(kd_i - \omega t_i)) \quad (5)$$

where  $wh$  is the wave height,  $k$  is the wavenumber,  $\omega$  is the angular frequency,  $d_i$  and  $t_i$  are the initial  $z$  position of the ion and total time, and  $d_f$  and  $t_f$  are the final  $z$  position of the ion and total time. The change in velocity due to the traveling wave was computed as

$$v_{z,new} = \sqrt{\frac{2 \left( \frac{1}{2} m_i v_z^2 + z \Delta V_{TW} \right)}{m_i}} \quad (6)$$

where  $v_z$  is the  $z$ -component of the velocity vector of the ion, if the quantity inside the square root was positive, and as

$$v_{z,new} = -\sqrt{\frac{2 \left| \frac{1}{2} m_i v_z^2 + z \Delta V_{TW} \right|}{m_i}} \quad (7)$$

if it was negative. Using this updated velocity, the velocity of the ion after the collision was computed as

$$\mathbf{v}_{new} = \sqrt{1-x} \left( -\mathbf{v} + \frac{m_i \mathbf{v} + m_g \mathbf{g}}{m_i + m_g} \right) + \frac{m_i \mathbf{v} + m_g \mathbf{g}}{m_i + m_g} \quad (8)$$

where  $x$  is the fraction of available kinetic energy converted to internal energy,  $\mathbf{v}$  is the velocity vector of the ion,  $\mathbf{g}$  is the velocity vector of the gas,  $m_i$  is the mass of the ion, and  $m_g$  is the mass of the gas. The change in internal energy due to the collision was computed as

$$\Delta U = \frac{x}{2} \mu (\mathbf{v} \cdot \mathbf{v} - 2\mathbf{v} \cdot \mathbf{g} + \mathbf{g} \cdot \mathbf{g}) \quad (9)$$

where  $\mu$  is the reduced mass, for the model with only a heating mechanism and no cooling mechanism, and as

$$\Delta U = \frac{x}{2} \mu (\mathbf{v} \cdot \mathbf{v} - 2\mathbf{v} \cdot \mathbf{g} + \mathbf{g} \cdot \mathbf{g}) - \frac{3}{n} U + \frac{1}{2} m_g v_g^2 - \frac{3}{2} k_b T_g \quad (10)$$

where  $U$  is the cumulative change in internal energy through the previous time step, for the model incorporating both heating and cooling mechanisms. After computing the change in internal energy the simulation advanced to the next time step.

If no collision occurred during a given time step, the change in velocity due to the traveling wave was determined as above and the simulation advanced to the next time step.

### Derivation of analytic expression for energy deposition in CIU without cooling

We determined an analytical expression for an extreme upper bound of energy deposition in CIU (i.e., in the absence of any cooling mechanisms) that is based on the kinetic theory of gases using the collision cross section of the ion.

For an ion-gas collision, the available center-of-mass-frame kinetic energy is given by

$$KE_{avail}^{CM} = \frac{1}{2} \mu \mathbf{v}_{rel}^2 = \frac{1}{2} \mu (\mathbf{v}_i - \mathbf{v}_g) \cdot (\mathbf{v}_i - \mathbf{v}_g) \quad (11)$$

where  $\mu$  is the reduced mass and  $\mathbf{v}_i$  and  $\mathbf{v}_g$  are the laboratory-frame velocity vectors of the ion and gas, respectively. Averaging over all possible  $\mathbf{v}_g$  gives

$$\langle KE_{avail}^{CM} \rangle = \frac{1}{2} \mu \langle (\mathbf{v}_i - \mathbf{v}_g) \cdot (\mathbf{v}_i - \mathbf{v}_g) \rangle \quad (12)$$

which simplifies to

$$\langle KE_{avail}^{CM} \rangle = \frac{1}{2} \mu (\langle \mathbf{v}_i^2 \rangle + \langle \mathbf{v}_g^2 \rangle) \quad (13)$$

or, in terms of kinetic energy

$$\langle KE_{avail}^{CM} \rangle = \frac{m_g \langle KE_i^{lab} \rangle}{m_i + m_g} + \frac{m_i \langle KE_g^{lab} \rangle}{m_i + m_g} \quad (14)$$

where  $m_i$  and  $m_g$  are the mass of the ion and gas, respectively, and  $\langle KE_i^{lab} \rangle$  and  $\langle KE_g^{lab} \rangle$  are the kinetic energies of the ion and gas, respectively. Let  $x$  be the fraction of available center-of-mass-frame kinetic energy converted to internal energy of the ion. Then the change in internal energy for a collision is

$$\langle \Delta U \rangle = x \left( \frac{m_g \langle KE_i^{lab} \rangle}{m_i + m_g} + \frac{m_i \langle KE_g^{lab} \rangle}{m_i + m_g} \right) \quad (15)$$

and the kinetic energy after the collision is

$$\langle KE_{post\ coll}^{CM} \rangle = (1 - x) \langle KE_{avail}^{CM} \rangle \quad (16)$$

Thus, the center-of-mass-frame velocities after the collision will be those prior to the collision reversed and scaled by  $\sqrt{1 - x}$ . Converting back to the laboratory frame we have

$$\mathbf{v}_{i,post\ coll} = \sqrt{1 - x} \left( -\mathbf{v}_i + \frac{m_g \mathbf{v}_i + m_i \mathbf{v}_g}{m_i + m_g} \right) + \frac{m_g \mathbf{v}_i + m_i \mathbf{v}_g}{m_i + m_g} \quad (17)$$

which simplifies to

$$\mathbf{v}_i^{post\ coll} = \mathbf{v}_i \left( \frac{m_g - m_i \sqrt{1 - x}}{m_i + m_g} \right) \quad (18)$$

Let  $a = \left( \frac{m_g - m_i \sqrt{1-x}}{m_i + m_g} \right)^2$ , then the kinetic energy of the ion after  $n-1$  collisions is

$$\langle KE_{i,n-1}^{lab} \rangle = \frac{1}{2} m_i \langle \mathbf{v}_{i,0}^2 \rangle a^{n-1} = \langle KE_{i,0}^{lab} \rangle a^{n-1} \quad (19)$$

and the internal energy after  $n$  collisions is

$$\langle \Delta U_n \rangle = x \left( \frac{m_g \langle KE_{i,n-1}^{lab} \rangle}{m_i + m_g} + \frac{m_i \langle KE_g^{lab} \rangle}{m_i + m_g} \right) \quad (20)$$

Substituting the expression for the kinetic energy of the ion from Eq. 18 gives

$$\langle \Delta U_n \rangle = x \left( \frac{m_g \langle KE_{i,0}^{lab} \rangle a^{n-1}}{m_i + m_g} + \frac{m_i \langle KE_g^{lab} \rangle}{m_i + m_g} \right) \quad (21)$$

The total change in internal energy is given by summing the change in internal energy for each collision

$$\langle \Delta U_{tot} \rangle = \sum_{n=1}^N \langle \Delta U_n \rangle = \sum_{n=1}^N x \left( \frac{m_g \langle KE_{i,0}^{lab} \rangle a^{n-1}}{m_i + m_g} + \frac{m_i \langle KE_g^{lab} \rangle}{m_i + m_g} \right) \quad (22)$$

where  $N$  is the number of collisions. Terms without  $n$  dependence can be moved outside the summation, yielding

$$\langle \Delta U_{tot} \rangle = \frac{N m_i x \langle KE_g^{lab} \rangle}{m_i + m_g} + \frac{m_g x \langle KE_{i,0}^{lab} \rangle}{m_i + m_g} \sum_{n=1}^N a^{n-1} \quad (23)$$

If  $N$  is large, then the total internal energy change can be expressed as

$$\langle \Delta U_{tot} \rangle = \frac{N m_i x \langle KE_g^{lab} \rangle}{m_i + m_g} + \frac{m_g x \langle KE_{i,0}^{lab} \rangle}{m_i + m_g} \frac{1}{1-a} \quad (24)$$

Substituting the expression for  $a$  and simplifying yields the final result

$$\langle \Delta U_{tot} \rangle = \frac{N m_i x \langle KE_g^{lab} \rangle}{m_i + m_g} + \frac{x(m_i + m_g) \langle KE_{i,0}^{lab} \rangle}{2m_i(1 + \sqrt{1-x}) + m_g x} \quad (25)$$

## Derivation of Model of Collisional Activation Capable of Both Heating and Cooling

The primary computational model for CIU described in the main text includes collisional heating as well as collision cooling of the ion due to interactions with the buffer gas. (Under the conditions used in these experiments, radiative cooling by emission of photons from the ions is much slower than collisional cooling.)

To derive a model that can both heat and cool the ions, we start with an protein ion with internal energy

$$U_{i,j-1} = \Delta U_{j-1} + nk_b T_{i,0} \quad (26)$$

where  $\Delta U_{j-1}$  is the cumulative change in internal energy at step  $j-1$ ,  $n$  is the number of modes,  $k_b$  is the Boltzmann constant, and  $T_{i,0}$  is the initial temperature of the ion. The ion has kinetic energy

$$KE_i^{lab} = \frac{1}{2} m_i v_i^2 \quad (27)$$

where  $m_i$  is the mass of the ion and  $v_i$  is the velocity of the ion. The gas has energy of

$$E_g = \frac{1}{2} m_g v_g^2 \quad (28)$$

where  $m_g$  is the mass of the gas and  $v_g$  is the velocity of the gas. The ion and gas form a collision complex with energy

$$E_{complex} = \Delta U_{j-1} + nk_b T_{i,0} + \frac{1}{2} m_g v_g^2 + \frac{3}{2} k_b T_g + \frac{x}{2} \mu (\mathbf{v}_i - \mathbf{v}_g) \cdot (\mathbf{v}_i - \mathbf{v}_g) \quad (29)$$

where  $x$  is the fraction of available center-of-mass frame kinetic energy converted to internal energy and  $\mu$  is the reduced mass. Note that the “extra”  $\frac{3}{2} k_b T_g$  of energy arises from bonding between the ion and gas. Assuming equipartition of energy, the total energy is distributed among  $n+3$  modes, so the gas atom carries away  $\frac{1}{2} \cdot \frac{3}{n+3}$  of the total energy as kinetic energy, and another  $\frac{1}{2} \cdot \frac{3}{n+3}$  goes into breaking the bonds. Thus, the internal energy of the ion after the collision is

$$U_{i,j} = \frac{n}{n+3} \left( \Delta U_{j-1} + nk_b T_{i,0} + \frac{1}{2} m_g v_g^2 + \frac{3}{2} k_b T_g + \frac{x}{2} \mu (\mathbf{v}_i - \mathbf{v}_g) \cdot (\mathbf{v}_i - \mathbf{v}_g) \right) \quad (30)$$

so the change in internal energy is

$$\begin{aligned} \Delta \Delta U_i &= \frac{n}{n+3} \left( \Delta U_{j-1} + nk_b T_{i,0} + \frac{1}{2} m_g v_g^2 + \frac{3}{2} k_b T_g + \frac{x}{2} \mu (\mathbf{v}_i - \mathbf{v}_g) \cdot (\mathbf{v}_i - \mathbf{v}_g) \right) - \Delta U_{j-1} \\ &\quad - nk_b T_{i,0} \\ &= \frac{1}{n+3} \left( \frac{1}{2} n m_g v_g^2 + \frac{3}{2} n k_b T_g + \frac{x}{2} n \mu (\mathbf{v}_i - \mathbf{v}_g) \cdot (\mathbf{v}_i - \mathbf{v}_g) - 3 \Delta U_{j-1} - 3 n k_b T_{i,0} \right) \quad (31) \end{aligned}$$

Assuming that the ion is initially thermalized to the temperature of the gas, i.e.  $T_{i,0} = T_g$ , this reduces to

$$\Delta\Delta U_i = \frac{1}{n+3} \left( \frac{1}{2} n m_g \mathbf{v}_g^2 - \frac{3}{2} n k_b T_g + \frac{x}{2} n \mu (\mathbf{v}_i - \mathbf{v}_g) \cdot (\mathbf{v}_i - \mathbf{v}_g) - 3\Delta U_{j-1} \right) \quad (32)$$

Since  $n$  is large, we have

$$\Delta\Delta U_i \approx -\frac{3}{n} (\Delta U_{j-1}) + \frac{1}{2} m_g \mathbf{v}_g^2 - \frac{3}{2} k_b T_g + \frac{x}{2} \mu (\mathbf{v}_i - \mathbf{v}_g) \cdot (\mathbf{v}_i - \mathbf{v}_g) \quad (33)$$

and the cumulative change in internal energy at step  $j$  is

$$\Delta U_j = \Delta U_{j-1} - \frac{3}{n} (\Delta U_{j-1}) + \frac{1}{2} m_g \mathbf{v}_g^2 - \frac{3}{2} k_b T_g + \frac{x}{2} \mu (\mathbf{v}_i - \mathbf{v}_g) \cdot (\mathbf{v}_i - \mathbf{v}_g) \quad (34)$$

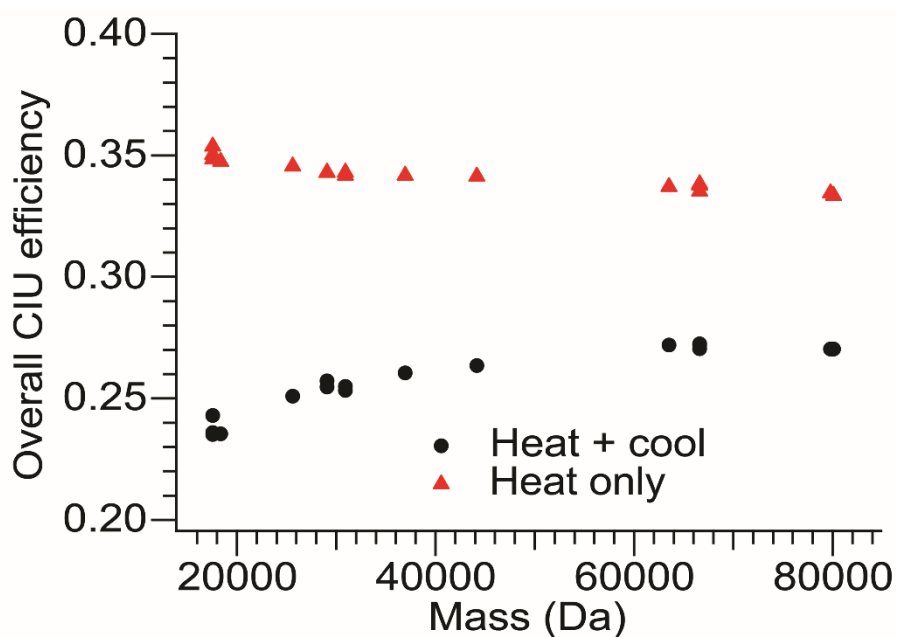


**Figure S2.** Computed overall CIU efficiency versus mass for each protein and charge state studied for models with heating only (red triangles) and heating and cooling (black circles). The addition of a cooling mechanism decreases the overall CIU efficiency by 20-30%. For the model with heating only the overall CIU efficiency decreases slightly with increasing mass, while for the model with heating and cooling there is a slight increase with mass, consistent with the prediction of longer cooling lifetimes for larger ions.

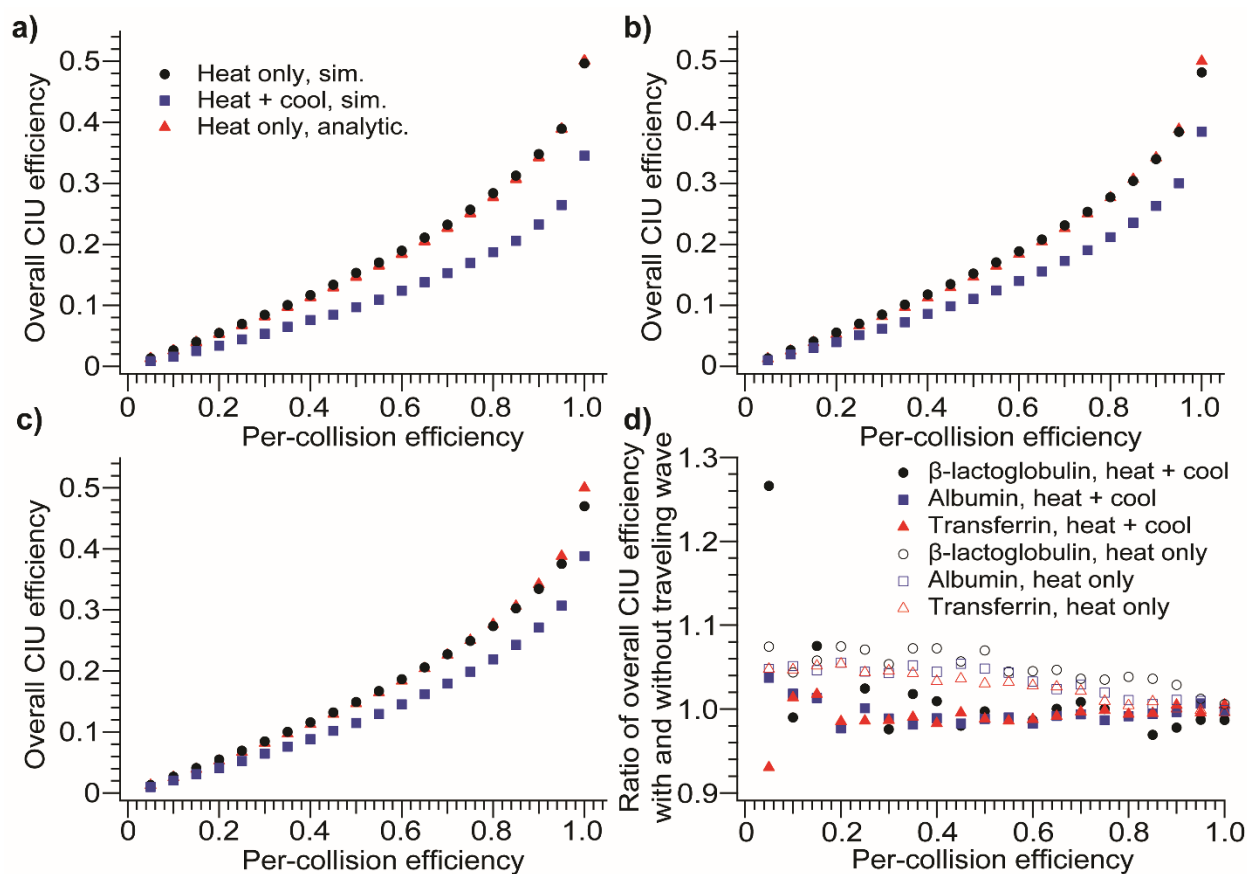


**Figure S3.** Comparison of overall CIU efficiencies determined from Monte Carlo simulations with (blue squares) and without (black circles) a cooling mechanism and those computed analytically (red triangles) at per-collision efficiency values ranging from 0.05 to 1 for **a)**  $\beta$ -lactoglobulin, 8+ **b)** albumin, 12+ **c)** transferrin, 18+. For all three proteins the values computed analytically and those derived from Monte Carlo simulations without cooling are nearly identical, and the addition of a cooling mechanism decreases the overall CIU efficiency. **d)** Effect of the traveling wave potential on the overall CIU efficiency. The ratio of the overall CIU efficiency with and without the traveling wave potential included is plotted against the per-collision efficiency. For the heating only model, the traveling wave increases the overall CIU efficiency by 5-8% at small to intermediate values of the per-collision efficiency, and has little effect at large values of the per-collision efficiency (we use a value of 0.9 to calibrate CIU data). For the model with heating and cooling, apart from very small (non-physical) values of the per-collision efficiency, the traveling wave has a negligible effect on the overall CIU efficiency.

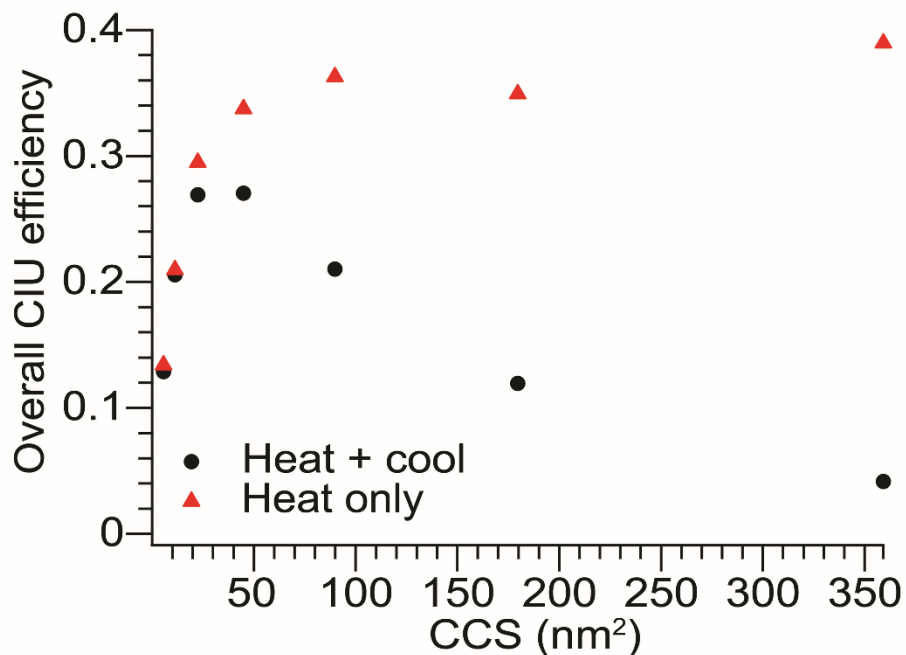


**Figure S4.** Computed overall CIU efficiency ( $\Delta U/zV$ ) for BSA<sup>15+</sup> for a wide range of CCS values using a heating only model (red triangles) and one with heating and cooling mechanisms (black circles). For the heating only model there is a rapid increase in the overall CIU efficiency followed by a plateau. As the number of collisions increases, each collision transfers a smaller amount of energy to internal modes, leading to the observed behavior. For the model with both heating and cooling, there is a similarly rapid increase for small CCS values, but the overall CIU efficiency peaks near the experimental CCS value and decreases at much larger CCS values due to increased cooling from the greater number of collisions.

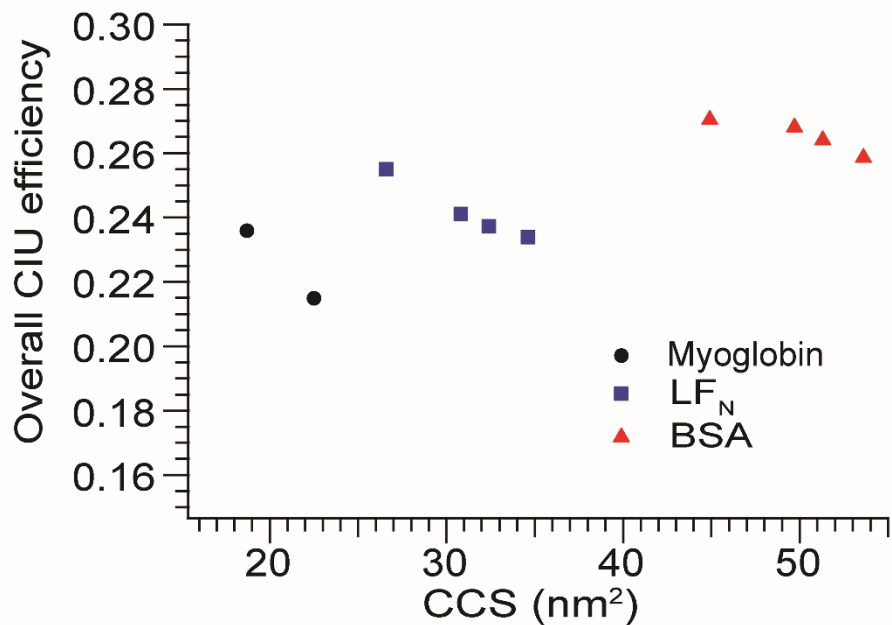


**Figure S5.** Computed overall CIU efficiency ( $\Delta U/zV$ ) for myoglobin<sup>7+</sup>, LF<sub>N</sub><sup>10+</sup>, and BSA<sup>15+</sup> for CCS values corresponding to experimentally determined conformer families. Increased CCS increases the number of collisions, slowing the ions down and simultaneously increasing the cooling rate. This leads to only a modest decrease in the overall CIU efficiency over the range of CCS investigated for each ion.

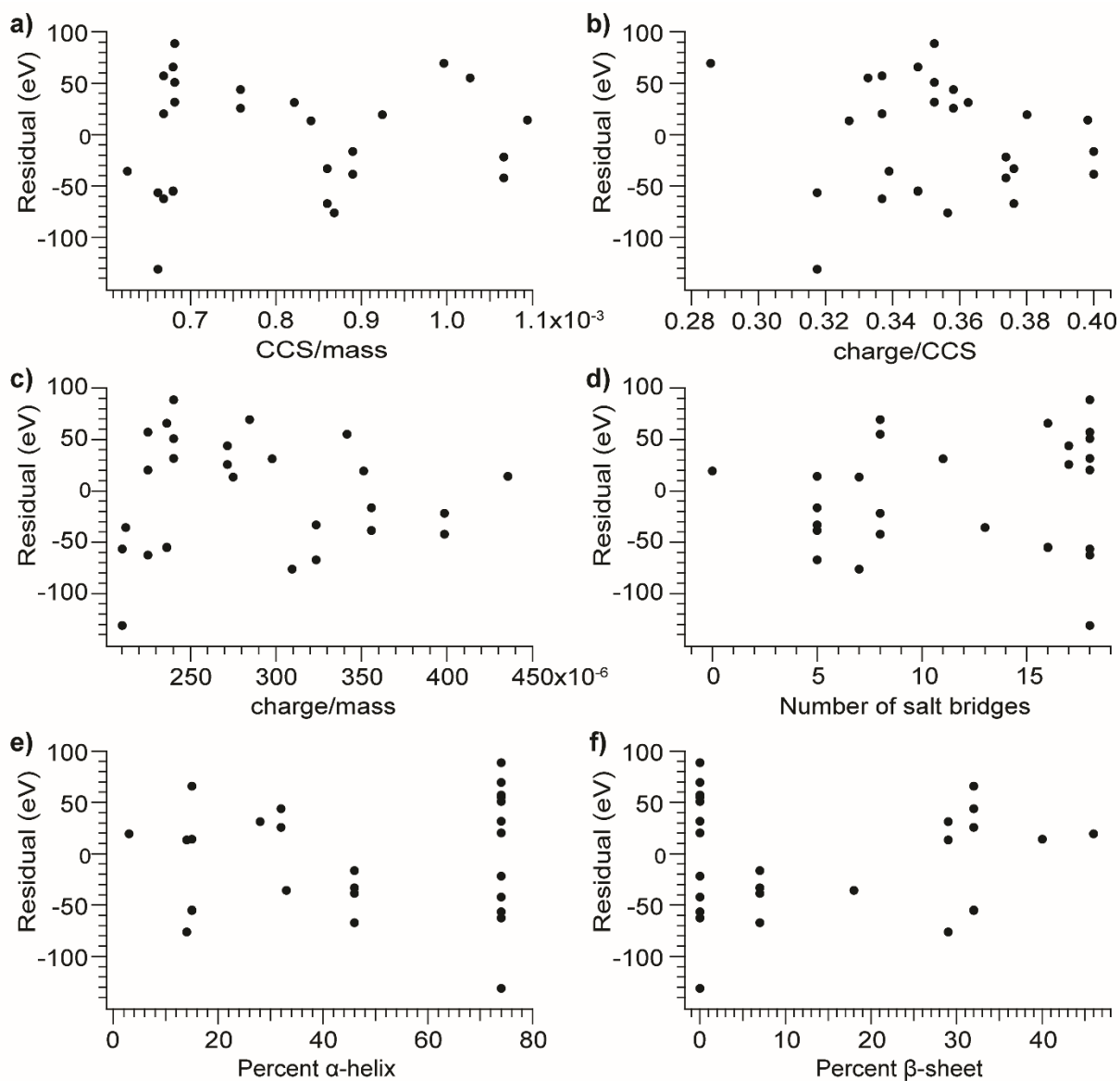


**Figure S6.** Plots showing relationship between residuals from power-law fit in Figure 2 and **a)** CCS divided by mass **b)** charge divided by CCS **c)** charge divided by mass **d)** number of salt bridges **e)** amount of  $\alpha$ -helical structure **f)** amount of  $\beta$ -sheet structure. In all six cases there is no correlation.

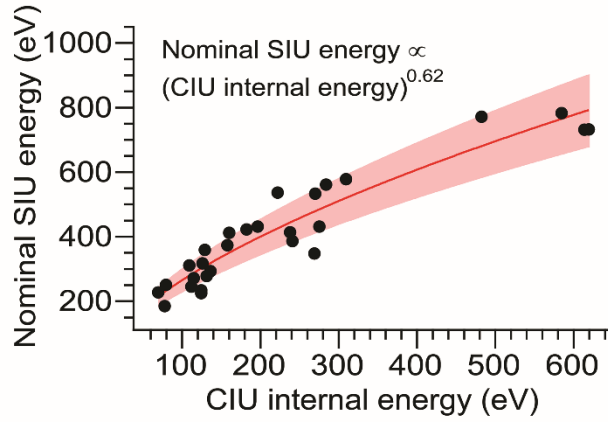


**Figure S7.** SIU appearance energy vs rescaled CIU internal energy, computed using the heating only model. The non-linear trend is fit to a power law relationship with an exponent of  $0.62 \pm 0.05$ . The shaded region represents  $\pm$  one standard deviation of the relative difference from the fit.

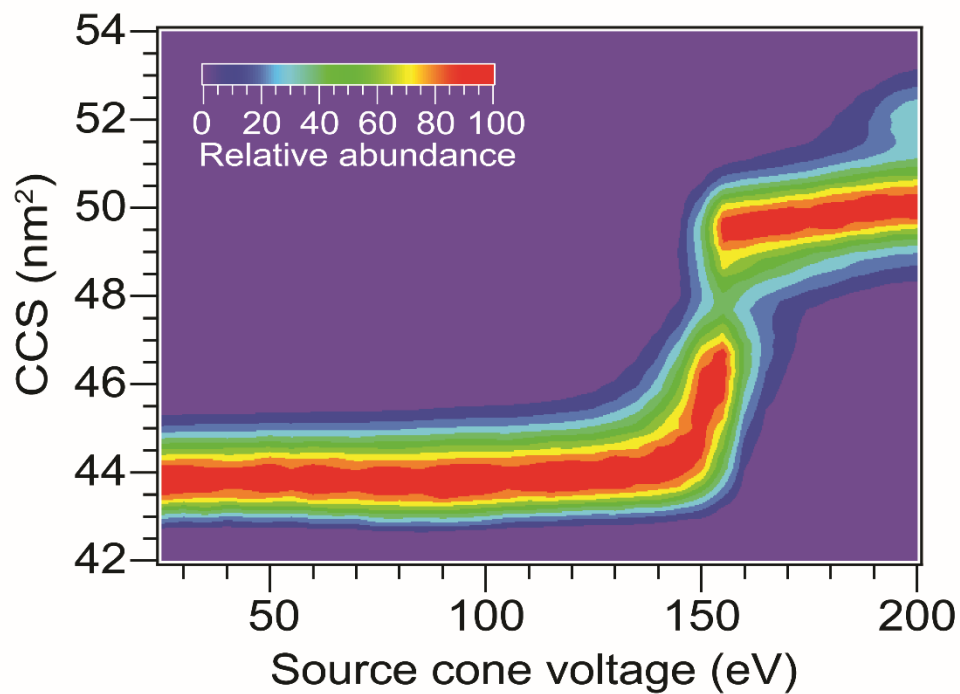


**Figure S8.** In-source unfolding of BSA<sup>15+</sup> at a backing pressure of 3.7 mbar. The unfolding transitions observed are the same as those produced by CIU in the Trap. However, the ions are activated less efficiently in the source region, requiring higher voltages to precipitate unfolding and leading to incomplete unfolding at the voltages accessible.

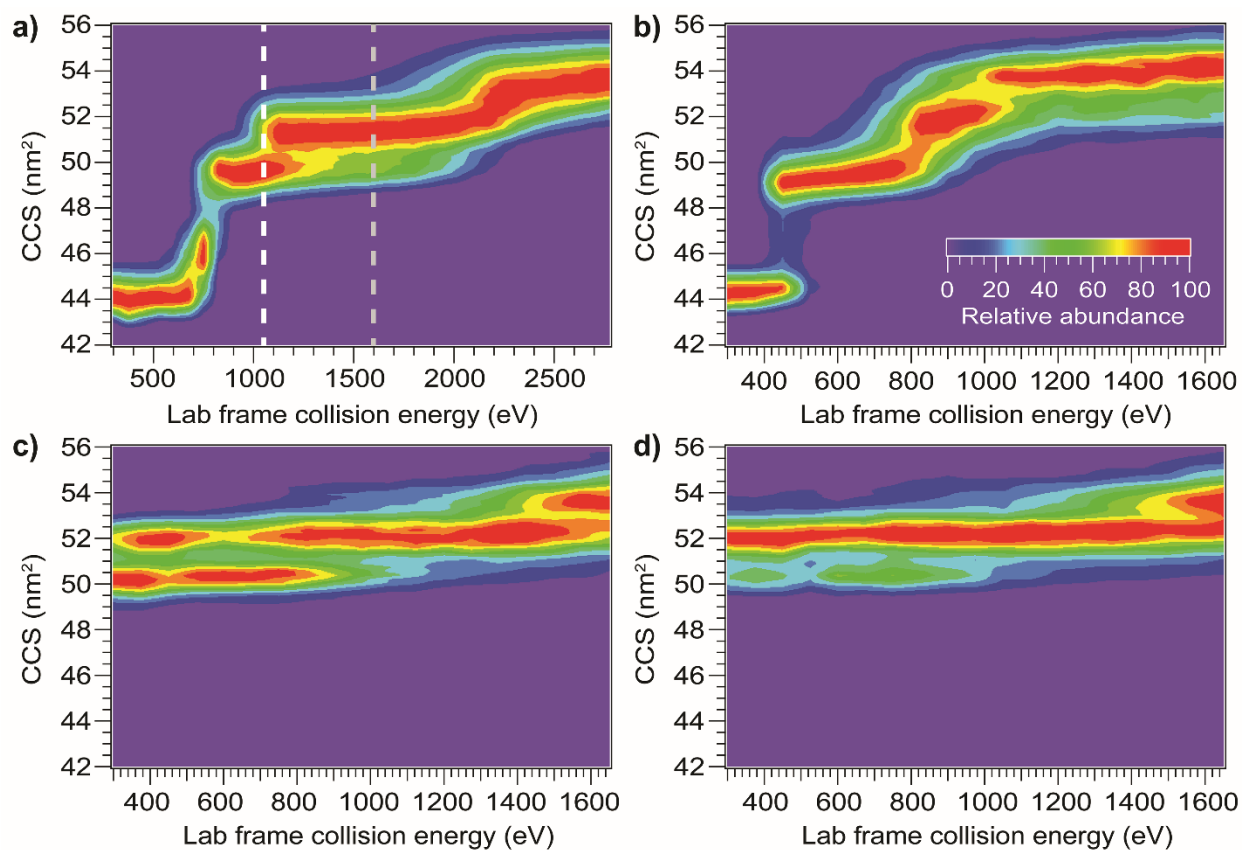


**Figure S9.** Effect of Trap pre-activation on SIU of BSA<sup>15+</sup>. **a)** CIU with dotted lines showing two different levels of Trap activation **b)** SIU with no Trap activation **c)** SIU following Trap activation to the white line in (a) requires significantly higher energies to cause further unfolding transitions **d)** SIU following Trap activation up to the gray line in (a) also requires significantly higher energies to cause further unfolding transitions

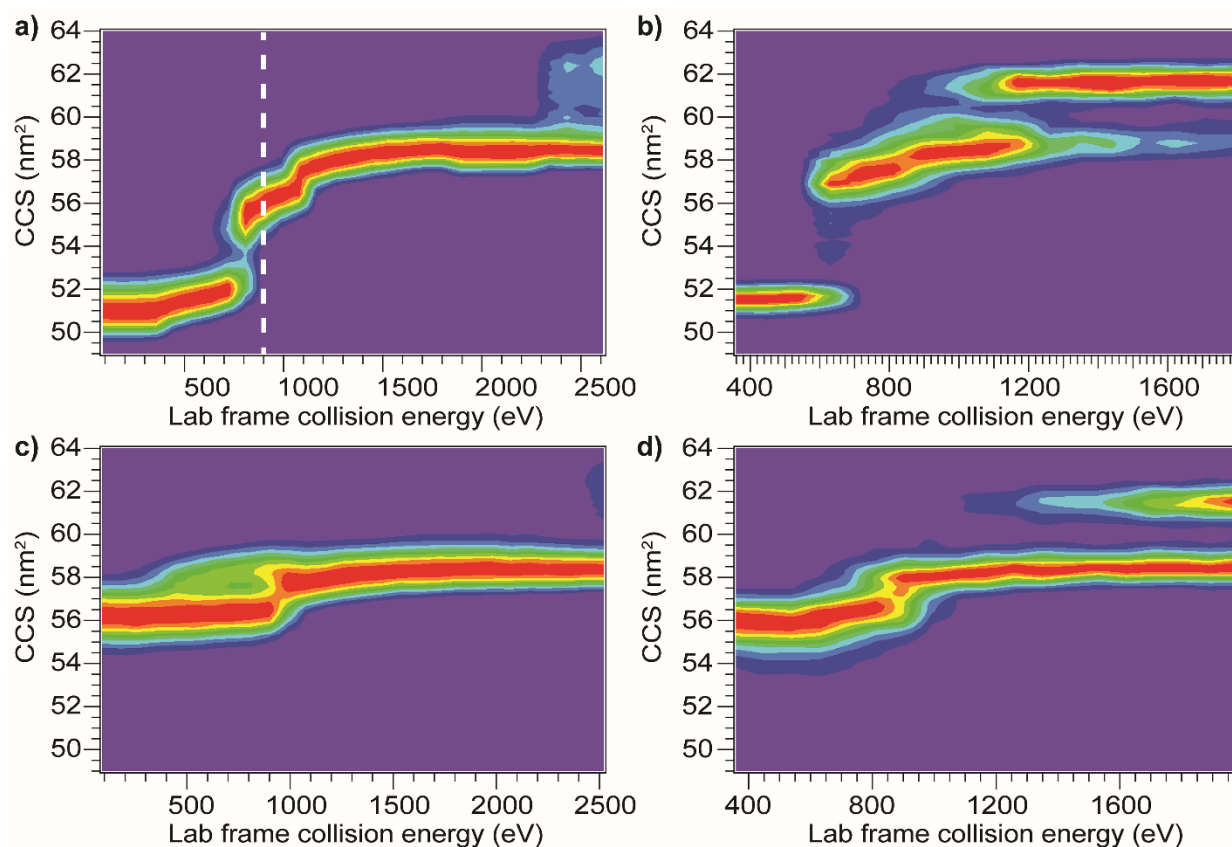


**Figure S10.** Effect of in-source pre-activation on CIU and SIU of  $\text{TF}^{18+}$ . **a)** CIU with no in-source activation and dotted line showing level of pre-activation in (c) and (d) **b)** SIU with no in-source activation **c)** CIU following in-source activation up to the dotted line in (a) exhibits a small shift to lower energy for the discontinuity at 1200 eV in (a) to 1000 eV in this experiment **d)** SIU following in-source activation up to the dotted line in (a) requires more energy to cause further unfolding

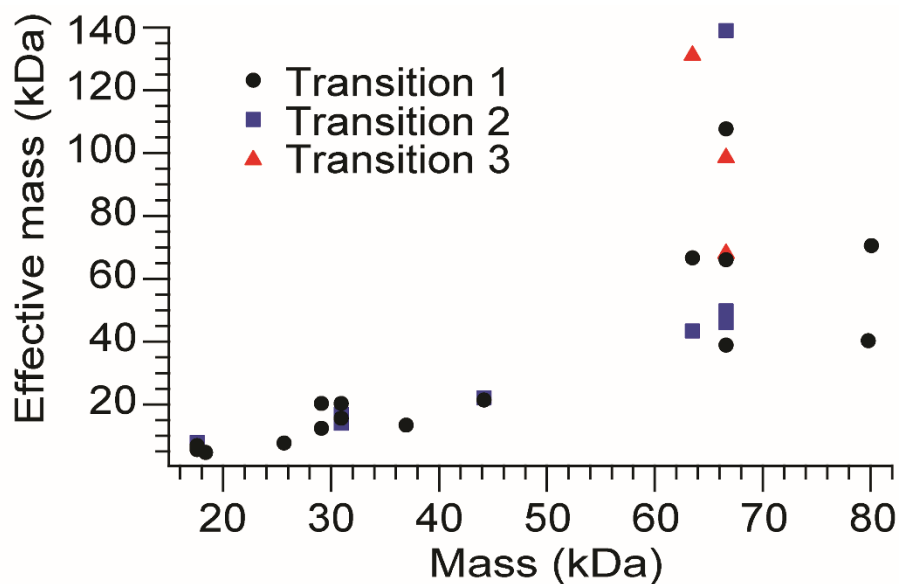


**Figure S11.** Effective mass of surface (see main text for definition) versus ion mass. For the first unfolding transition, the effective mass of the surface grows roughly linearly with ion mass. However, the effective mass of the surface can be much higher for the second and particularly the third unfolding transition. These transitions occur at higher energies and suggest that the ion-surface interaction depends on the kinetic energy of the ion.